Journal of Materials Chemistry C

Accepted Manuscript

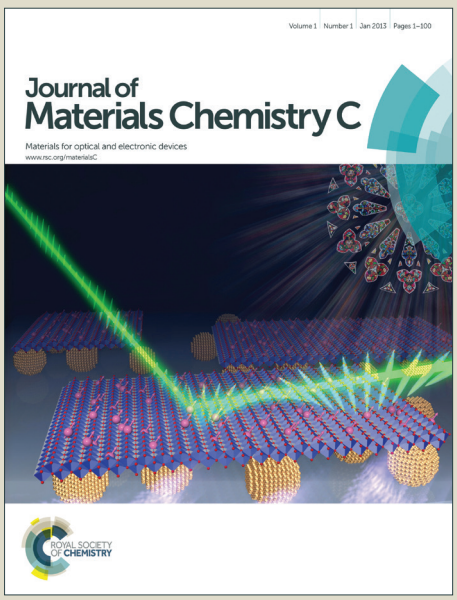

ROYAL SOCIETY OF CHEMISTRY

www.rsc.org/materialsC

Cite this: DOI: 10.1039/c0xx00000x

www.rsc.org/xxxxxx

ARTICLE TYPE

Highly Efficient Field Emission Properties of Novel Layered VS_2/ZnO Nanocomposite and Flexible VS_2 Nanosheet

Changqing Song,[a,b] Ke Yu,*[a] Haihong Yin,[a,b] Hao Fu,[a] Zhengli Zhang,[a] Ning Zhang [a] and Ziqiang Zhu[a]

Received (in XXX, XXX) Xth XXXXXXXXX 20XX, Accepted Xth XXXXXXXXX 20XX

DOI: 10.1039/b000000x

Multi-layered VS_2 nanosheets were synthesized via a facile hydrothermal process without using any additives or surfactants. Because of the large quantities of sharp edges, VS_2 nanosheet can serve as an efficient edge emitter for field emission (FE). FE properties of VS_2 nanosheet were investigated for the first time. The results indicated that VS_2 nanosheet had excellent field emission performance with turn-on field of ~1.4 $V\mu m^{-1}$ and threshold field of ~2.6 $V\mu m^{-1}$ on Si substrate. Moreover, FE properties of ZnO-coated VS_2 nanosheet were also investigated. VS_2/ZnO nanocomposite showed enhanced field emission properties with turn-on field of ~1.2 $V\mu m^{-1}$ and threshold field of ~2.2 $V\mu m^{-1}$, as well as the excellent emission stability without significant current degradation, which resulted from well contacted metal-semiconductor junction and extra emission sites. In addition, the FE properties of VS_2 nanosheet were preserved on the highly flexible polyethylene terephthalate (PET) substrate. Approximately the same value of turn-on field (~1.8 $V\mu m^{-1}$) and threshold field (~3.2 $V\mu m^{-1}$) were measured on bent or unbent PET substrates.

1. Introduction

Field emission(FE) is a quantum mechanical tunneling phenomenon in which electrons emit to vacuum from a solid surface due to the presence of an external electric field.[1] Compared with thermionic emission, field emission attracts more attention because of its fast turn-on process, low working temperatures and miniaturized device size,[2] and is widely used in a kind of vacuum electronic applications such as high energy accelerators, X-ray generators, flat panel displays, and microwave amplifiers.[3, 4] In early research, field emission properties of many one-dimensional (1D) nanomaterials (for example, ZnO, SnO_2, In_2O_3, CuO, TiO_2, and carbon,[5-7] etc.) have been widely performed due to their high surface-to-volume ratio and special morphology such as nanowires, nanotubes, nanorods, and nanotips. Since the discovery of the excellent field emission properties of two-dimensional (2D) graphene material in 2004,[8] a series of 2D and 2D-based graphene nanostructures have attracted tremendous attention in field emission studies in the past few years.[9-13] Although graphene is the most well known layered material, newly-rising interest has occurred in many layered transition metal dichalcogenides (TMDs), such as MoS_2, WS_2, VS_2 and TiS_2, for their various physical and chemical properties. Among them, VS_2 crystal is consisted of a metal V layer sandwiched between two S layers, with these triple layers stacking together to form a layered structure.[14] Recently, in the first principle theory calculation and experiments performed by Mulazzi and Feng et al.,[15, 16] 2D layered VS_2 nanomaterials showed excellent electrical conductance, high aspect ratio, ultrathin edges, and good mechanical properties. These characteristics satisfy the requirements for a good field emitter perfectly.[3] Thus, encouragingly, we considered that, in contrast to these conventional field emission materials mentioned above, 2D VS_2 nanocrystal may be a potential and competitive candidate for applications in field emission devices.

Although bulk VS_2 was first successfully synthesized in 1970s,[17] the synthesis and application researches of layered VS_2 were hampered because of the toxic synthetic processes and exfoliation difficulty.[18, 19] Recently, Feng et al.[20] reported a facile all-in-solution route to synthesize flexible VS_2 thin nanosheet for the first time, taking an intermediate of $VS_2{\cdot}NH_3$ as precursors, which avoided toxic synthesis and exfoliation difficulty. This promoted the study of layered VS_2 nanomaterial, such as the supercapacitor and ferromagnetism.[21] In this work, phase-pure hexagonal VS_2 layer crystals were firstly synthesized via a convenient hydrothermal method, and then their FE properties were detailedly investigated for the first time. The results indicated that the 2D layered VS_2 crystals own excellent field emission performance on Si substrate and the values are better than those we reported on multiwall CNTs emitters.[5] Moreover, the FE properties of VS_2/ZnO nanocomposite were also investigated. The result shows a better emission performance than that of the VS_2 emitters. In addition, flexible display technology has attracted considerable attention in recent years.[22, 23] As a newly emerging 2D flexible material, we investigate the flexible FE properties of VS_2 nanosheets. They were deposited onto a flexible PET film by Au sputtering to constitute a mechanically stretchable and electrical conductive substrate. The result shows almost the same field emission performance in both bent and unbent conditions based on PET substrates, which offers a new

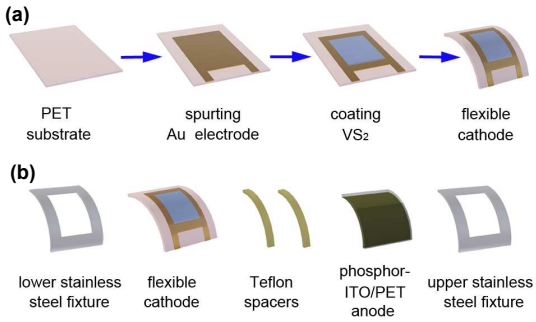

Fig. 1 (a) A schematic illustration of the fabrication process of a flexible cathode based on PET substrates. (b) Schematic illustrations of the parts of measurement structure for flexible FE properties under convex condition.

avenue for controllable field emitters in flexible applications. To our knowledge, this is the first study on the FE properties of layered VS_2 nanocrystal and VS_2/ZnO nanocomposite, which clearly suggests that the layered VS_2 nanocrystal is a competitive material in FE applications and the improved FE properties could be related to the decrease of potential energy barrier at the interface of VS_2 and ZnO.

2. Experimental Methods

2.1 Synthesis of layered VS_2 nanosheets

Layered VS_2 synthesis was performed using a modified hydrothermal procedure[20]. All the chemical reagents used in this experiment were analytical grade and used without further purification. In brief, 3 mmol of $Na_3VO_4 \cdot 12H_2O$ powder and 15 mmol of thioacetamide powder were added into 80 mL deionized water. The solution was stirred for 30 min to form homogeneous solution and then transferred into a 100 mL Teflon-lined stainless-steel autoclave. The autoclave was sealed and maintained at 160 ℃ for 24 h and then air-cooled to room temperature. The resulting dark precipitates were collected and washed with ethanol twice and then deionized water several times without being dried. After that, the above precipitates were ultrasonicated in iced water for 60 min. The resultant dark suspension was allowed to stand still for 24 h in a sealed beaker. Then, the upper part of the suspension was sucked and kept in wild-mouth bottle. Approximately half of the sucked suspension was centrifuged and dried in vacuum at 60 ℃ for 6 h. Thus, layered VS_2 nanosheets were obtained. The other sucked suspension was kept for the following step.

2.2 Synthesis of the ZnO nanoparticles

ZnO nanoparticles were also fabricated via a hydrothermal method. Traditionally, 10 mL of a urea solution (2 M) was added dropwise into 10 mL of a zinc chloride solution (0.5 M), which was then dissolved in 80 mL of deionized water. The mixture was stirred continuously for 30 min under room temperature and then transferred into an autoclave and maintained at 140 ℃ for 6 h. After the reaction, the product was washed in a centrifuge with ethanol and deionized water several times at 80 ℃ to remove any impurities. Finally, ZnO nanoparticles were obtained and kept in deionized water.

2.3 Synthesis of the VS_2/ZnO binary nanocomposite

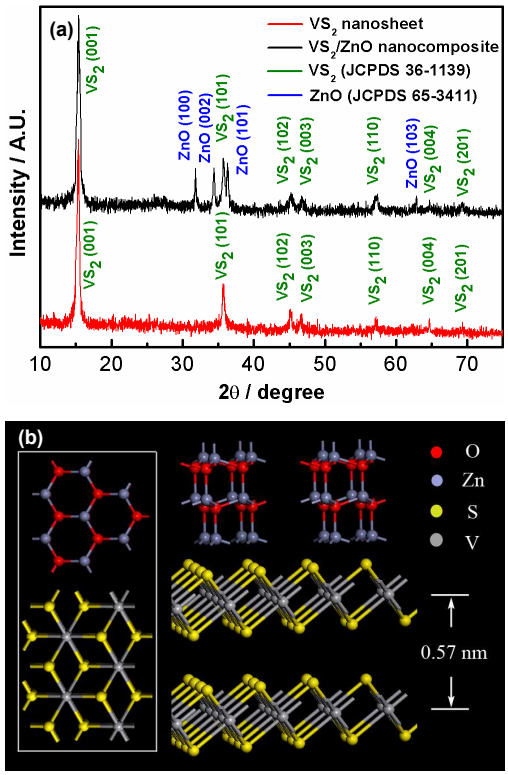

Fig. 2 (a) X-ray diffraction patterns of VS_2 nanosheets (red curve) and VS2/ZnO binary nanocomposite (black curve). (b) Schematic showing the atomic structures of ZnO and VS_2 (side view). Left insert is the top view of the corresponding structures.

A small amount of the as-synthesized ZnO nanoparticles were combined into the as-prepared VS_2 suspension. The solution was ultrasonicated and stirred for 1 h. After that, the deposition was collected and dried in vacuum at 60 ℃ for 6 h and treated with a thermal annealing process (300 ℃, 30 min, argon atmosphere), which has a function of facilitating the combination of VS_2 nanosheets and ZnO nanoparticles. Therefore, the VS_2/ZnO nanocomposites were obtained.

2.4 Sample characterization

The crystal morphology and structure of the resulting products were characterized by field emission scanning electron microscopy (FESEM, JEOL-JSM-6700F) at an accelerating voltage of 20 kV, atomic force microscope (AFM, Digital Instruments Dimension 3100, Veeco) with the tapping mode，X-ray diffraction (XRD, Bruker D8 Advance diffractometer) with Cu-Kα radiation(λ=1.5418 Å) and transmission electron microscopy (TEM, JEOL-JEM-2100) at an accelerating voltage of 200 kV. Ultraviolet Photoelectron Spectroscopy (UPS) experiments were carried out on a Shimadzu Axis Ultra electron spectrometer using He (I) ultraviolet light (21.21 eV) as the excitation source.

2.5 Field-emission measurement

Si substrate and flexible PET substrate were used for field emission investigation. For Si substrate, VS_2 nanosheets, VS_2/ZnO binary nanocomposite and ZnO nanoparticles were investigated respectively. The synthesized samples of VS_2 nanosheets and VS_2/ZnO binary nanocomposite were prepared on

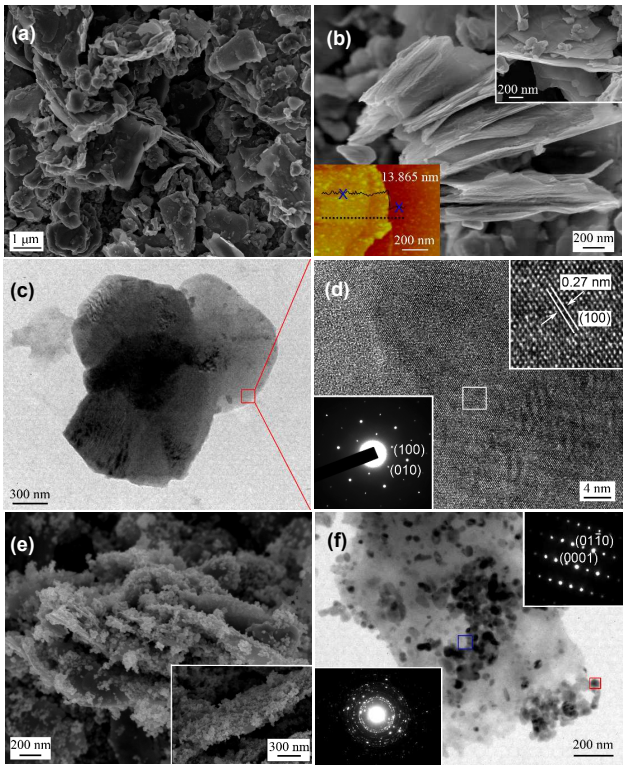

Fig.3 (a) Low-maginification SEM image for the VS_2 nanosheets synthesized at 160 ℃. (b) High-magnification SEM image of multi-flake layered VS_2 nanosheets. Upper inset is the high magnification SEM image of few flack layered VS_2 nanosheets. Lower inset is the AFM image of a VS_2 nanosheet with the tapping mode. (c) TEM image of VS_2 samples. (d) High- resolution TEM image for a selected area marked within a red rectangle from a nanosheet (Fig. 3c). Upper inset is an HRTEM image corresponding to a selected area marked within a white rectangle. Lower inset is the corresponding SAED pattern. (e) SEM image of ZnO-coated VS_2 nanosheets. (f) TEM image of VS_2/ZnO Nanocomposites. Upper inset is the corresponding SAED pattern of a ZnO nanopartical to a selected area marked within a red rectangle. Lower inset is the corresponding SAED pattern of the nanocomposite within a blue rectangle.

the silicon substrates by deposition, respectively. After that, they were dried in vacuum at 60 ℃ for 6 h. The ZnO sample was painted on the silicon substrates by screen-printing method. The silicon substrate with nanomaterial (as a cathode) was separated from a phosphor–ITO/PET anode with a distance maintained at 400 μm by Teflon spacers. As a comparison, a flexible PET substrate was also used for FE investigation under convex, concave and unbent conditions, respectively. VS_2 nanosheets were firstly deposited on a PET substrate with a thin Au film (~30 nm) and the schematic illustration was shown in Fig. 1(a). Then, the flexible cathode was separated from a phosphor–ITO/PET anode by Teflon spacers with thickness of 400 μm, and fixed with a set of stainless steel fixture. These parts are shown in Fig. 1(b), (convex condition). The curvature radius of the stainless steel fixture was 50 mm. For the concave and unbent conditions, we changed the direction of stainless steel fixture and used a flat stainless steel fixture to perform the measurement, respectively. Field emission properties were measured with a high vacuum level of about 2×10^{-5} Pa at room temperature using transparent anode imaging technique. The measured emission

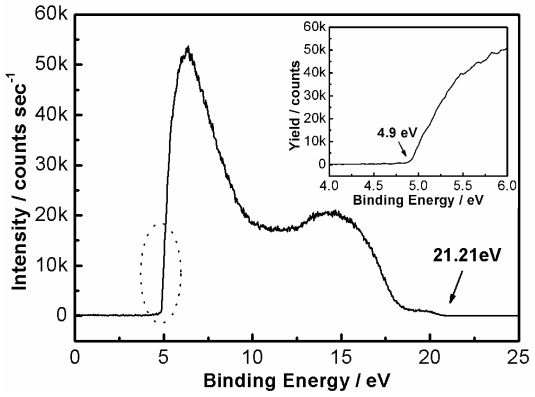

Fig. 4 UPS spectra of the VS_2 nanosheets. Inset shows an expanded view for the region marked in dotted eclipse.

area was 1×1 cm^2. In the measurement, the turn-on field is determined as the field produces a current density of 1μAcm^{-2}, and the threshold field is the field that produces a current density of 0.1mAcm^{-2}.

3. Results and discussion

3.1 Structure and morphology

Fig. 2a shows the XRD patterns of the VS_2 nanosheets and VS_2/ZnO binary nanocomposite. All the peaks in Fig. 2a (red curve) could be clearly indexed to the pure hexagonal phase of VS_2 (JCPDS 36-1139) with lattice constants of a =b= 0.3218 nm and c = 0.5755 nm. No peaks for other impurities were found in the spectra. This indicates that pure crystalline VS_2 was formed via the hydrothermal process. Furthermore, the sharp and narrow peaks indicate that the nanostructures are highly crystallized. The XRD pattern for VS_2/ZnO nanocomposite is shown in Fig. 2a (black curve), which exhibited the characteristic peaks for the wurtzite structure of ZnO (JCPDS 36-1451). In the nanocomposite diffractogram, distinct lattice planes corresponding to the ZnO nanoparticles and VS_2 nanosheets revealed the presence of individual components of ZnO and VS_2. The schematic crystal structures of VS_2 and ZnO were showed in Fig. 2b. The sandwiched structure of VS_2 crystal was stacked together by weak van der Waals interactions with an interlayer spacing of 0.57 nm. ZnO nanoparticles adhered to the surface of VS_2 nanosheet. We consider the combination of VS_2/ZnO nanocomposite due to the nano-reunion.[24, 25]

The morphology of the as-prepared product was observed by scanning electron microscopy (SEM) and transmission electron microscopy (TEM). A set of SEM images at different magnifications are shown in Fig. 3a and b. Macroscopically, as shown in Fig. 3a, it is apparent that the pristine layered VS_2 sample comprising flat particles with an average diameter of 0.5 to 2 μm are well-dispersed. The typical surface morphology of the nanosheets could be clearly observed in Fig. 3b and the upper inset in Fig. 3b, possesses a 2D multi-nanosheet or few nanosheet assembled pattern with sharp edges. Furthermore, a typical tapping mode AFM image of VS_2 nanosheet is shown in the lower inset of Fig. 3b. The thickness of the nanosheet is 13.865nm. These nanosheet-assembled structures with sharp edges are very effective to improve the field emission properties.

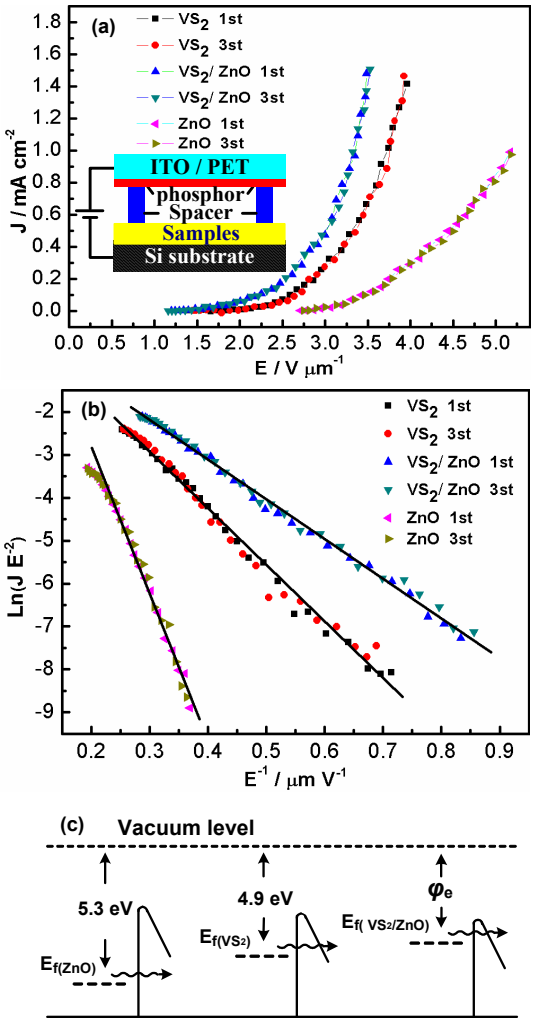

Fig. 5 (a) The dependence of the FE current density J on the applied electric field strength E of VS_2 nanosheets, ZnO nanoparticles and VS_2/ZnO nanocomposite, respectively. The inset is the schematic illustration for FE measurement. (b) The corresponding Fowler–Nordheim relation of $\ln(JE^{-2})$ − E^{-1} plots for these three types of samples. (c) Schematic diagrams of edge states and corresponding energy band of these three samples, respectively.

To further investigate the morphology and crystallographic features of the VS_2 nanosheets, TEM and HRTEM measurements were performed (Fig. 3c and d). Fig. 3c shows a TEM image of the VS_2 architectures, which were constructed from thin nanosheets. The high-resolution TEM image and the corresponding selected-area electron diffraction(SAED) pattern from the platelet of the nanosheets (Fig. 3c , square region marked in red) are shown in Fig. 3d, indicating that the nanosheet is single crystal, and the lattice spacing is 0.27 nm according to the periodic pattern in the lattice fringe image, corresponding to the (100) plane of VS_2 nanosheets.

The morphology and microstructure of the as-prepared VS_2/ZnO binary nanocomposites were also examined by FESEM and TEM. The results of which are shown in Fig. 3e and f. Fig. 3e and the inset shows the high-magnification SEM images of the as-prepared multi-sheet and few sheet assembled VS_2/ZnO binary structure. It is observed that for the VS_2/ZnO nanocomposites, the VS_2 nanosheets are covered with spherical ZnO nanoparticles in

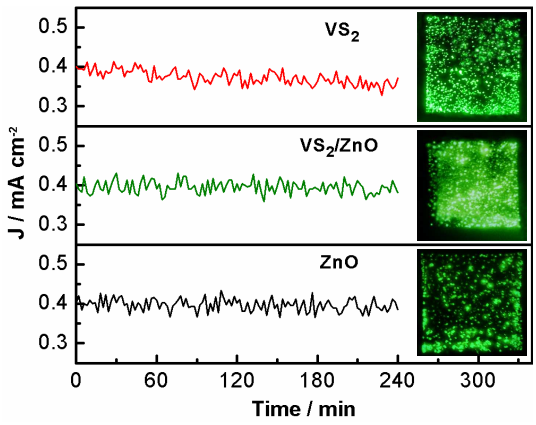

Fig. 6 Emission stability for VS_2 nanosheets, ZnO nanoparticles and VS_2/ZnO nanocomposite with original emission current density of 0.4 $mAcm^{-2}$. Inset is the field emission photos for these three samples, respectively (right).

high densities and the sizes of them are within the average range of 20 to 30 nm. As can be seen from Fig. 3f, TEM views of the ZnO nanoparticles adhered to the VS_2 nanosheets. Upper and lower insets of Fig. 3f show the selected area electron diffraction (SAED) patterns of a single ZnO nanoparticle (red rectangle) and nanocomposite (blue rectangle) of this sample respectively. The upper SAED pattern reveals that the ZnO nanoparticle is effectively a single crystal with preferred growth along the [0001] direction. The diffraction spots from the lower partten confirms the co-existence of ZnO nanoparticles and VS_2 nanosheets. Polycrystalline rings result from ZnO nanoparticles and single crystal spots, from VS_2 nanosheets.

In order to confirm the contribution of VS_2 nanosheet for field emission properties, work function of these VS_2 nanosheet was investigated by UPS analysis. Fig. 4 shows the corresponding UPS spectra at room temperature. It can be seen clearly that the value of work function is about 4.9 eV.

3.2 Field emission study of layered VS_2/ZnO nanocomposite

Field emission properties of the as-prepared samples were measured by the method described in the experimental section. Herein, we studied the field emission properties of both the VS_2 nanosheets and VS_2/ZnO binary nanocomposites at room temperature for the first time. Fig. 5a shows the characteristic emission current density versus applied electric field on Si substrate. The turn-on and threshold fields for the ZnO nanopartical are 2.7 and 3.5 $V\mu m^{-1}$. For VS_2 nanosheet and VS_2/ZnO binary nanocomposite, the turn-on and threshold fields are 1.4 and 2.6 $V\mu m^{-1}$, 1.2 and 2.2 $V\mu m^{-1}$, respectively. Intriguingly, it is shown that the field emission property for the VS_2 nanosheet emitters is better than that of the multiwall CNTs and compares favorably with various graphene nanostructural emitters[5, 26]. Moreover, the field emission property for the VS_2/ZnO binary nanocomposite emitters has been significantly improved in comparison with that of the VS_2 nanosheet.

The Fowler–Nordheim (F–N) plots corresponding to the data in Fig. 5a are shown in Fig. 5b. It is interesting that the F–N plots of all these three samples are in straight lines, which indicates that the emitting electrons are mainly resulted from barrier tunneling electrons extracted by the electric field. The field emission characteristic can be expressed by the Fowler– Nordheim (F–N)

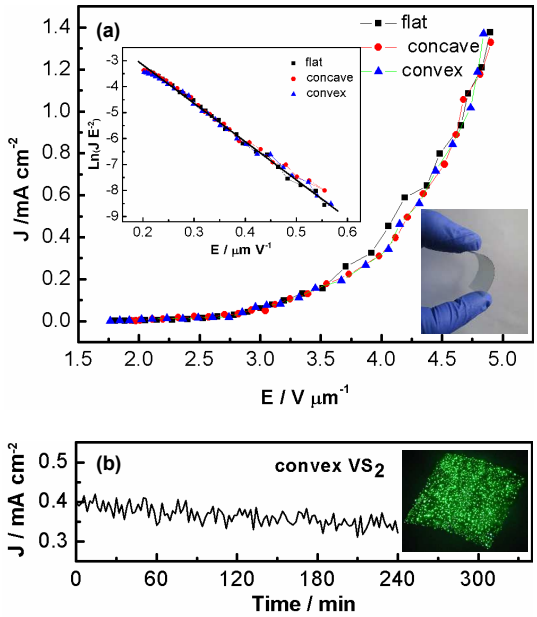

Fig. 7 (a) J-E plots of field emission properties measured in flexible substrates. Upper inset is the corresponding F-N slops. Lower inset is the photo of VS_2 nanosheets coating on flexible PET substrate. (b) Emission stability for convex sample with original emission current density of 0.4 $mAcm^{-2}$. Inset is the corresponding field emission photo (right).

equation:

$$\ln(J/E^2) = (1/E)(-B\phi^{3/2}/\beta) + \ln(A\beta^2/\phi) \quad (1)$$

where J is the emission current intensity, E is the applied electric field, A and B are constants with the values of 1.56×10^{-10} $AV^{-2}eV$ and 6.83×10^{3} $eV^{-3/2}V\mu m^{-1}$, β is the field enhancement factor, φ is the work function of the emitter material. According to equation (1), the slope of the F–N plots has an inverse ratio to the field enhancement factor β and can be listed as follows

$$k_{slope} = -B\phi^{3/2}/\beta \quad (2)$$

On the basis of the early research, the work function of ZnO is 5.3 eV.[27] From the slopes of F–N plots, the field enhancement factor β for ZnO nanoparticles and VS_2 nanosheets are obtained to be 2216 and 5588, respectively.

Generally, field emission mainly depends on the emitter geometry, crystal structure, and the spatial distribution of emitting centers[28-30]. The VS_2 nanosheets have lower work function and higher aspect ratio. Therefore, it is reasonable that electrons can be emitted more easily from these sharp edges in comparison with the ZnO nanoparticles. For VS_2/ZnO binary nanocomposite, it is believed that the better field emission property than VS_2 nanosheet is correlated with not only the high field enhancement factor of the emitters but also the tunneling effect of electrons through VS_2-ZnO junction. Considering the work functions of VS_2 and ZnO with about 4.9 eV and 5.3 eV, respectively, when they come into contact, there is a formation of a metal-semiconductor junction at their interface. In order to achieve thermal equilibrium in this junction with different work functions, electrons will flow from VS_2 nanosheets to the ZnO nanoparticles and gather on the surface of the ZnO nanoparticles. Since ZnO nanoparticles were undoped, we consider it a non-rectifying barrier for the junction between VS_2 nanosheets and ZnO nanoparticles.[22] With a low resistance contact between VS_2 nanosheets and ZnO nanoparticles, the barrier of resistance on the VS_2-ZnO junction was removed and electrons were easily injected from the Fermi level of VS_2 into the conduction band of ZnO under external electric field. The electrons in the conduction band of ZnO are emitted to the vacuum through subsequent F–N tunneling under strong local electric field.[31, 32] Moreover, previous reports indicate that the enhancement factor would be dramatically increased by multistage geometry.[33] In the case of our VS_2/ZnO nanocomposite, the applied primary field gets enhanced on the VS_2 nanosheets, which successively act as a secondary field for the ZnO nanoparticles, thereby enhancing the local electric field. In addition, the ZnO nanoparticles on the surface of VS_2 nanosheets can act as extra emission sites and increase the number of emission dots because of their small sizes which improve their field emission property. That is to say, VS_2/ZnO nanocomposite owns lower effective work function (φ_e).[34] We exhibit the schematic edge states and corresponding energy band diagrams of the electron emission to vacuum from these three samples in Fig. 5c to show the φ_e of VS_2/ZnO nanocomposite. For these reasons, VS_2/ZnO nanocomposite shows excellent field emission properties.

Current stabilities of ZnO nanopartical, VS_2 nanosheet and VS_2/ZnO nanocomposite emitters are also investigated. The current stability curves of them are given in Fig. 6 by plotting the emission current density versus a function of time with original emission current density of 0.4 $mAcm^{-2}$. For these three field emission sources, no obvious degradation of current density was observed during 4 h for ZnO nanopartical and VS_2/ZnO nanocomposite. As revealed in Fig. 6, the emission for the VS_2/ZnO nanocomposite emitters was more stable than VS_2 nanosheets, which could be attributed to the fact that ZnO has excellent chemical stability and can protect the emitter from ion bombardment during operation.[32] Thus, a high field emission current stability is sustained for the VS_2/ZnO nanocomposite. The inset of Fig. 6 shows the field emission images of these three emitters operated at an electric field of 3.2 $V\mu m^{-1}$. The emission spot density for the VS_2/ZnO nanocomposite emitters is about 10^4 cm^{-2}, which is obviously higher than that of the VS_2 and ZnO emitters. Also the light spots on the fluorescent screen became more uniform and denser. The improvement of the light emitting quality can be attributed to the large number of ZnO nanoparticles, which serve as emitters on the surface of the VS_2 nanosheets.

3.3 Field emission properties of flexible VS_2 nanosheet

The mechanically flexible, electro-conductive VS_2/Au/PET substrate was shown in the lower inset of Fig. 7a. To investigate the FE properties on flexible substrate of VS_2 nanosheets, we bent the PET substrate coated with VS_2 samples several times before test. The radius of curvature of PET substrate is about 50mm. Fig. 7a shows the characteristic emission current density versus applied electric field on PET substrate for states of flat, concave and convex films, respectively. In the flat sample configuration, the turn-on fields and threshold fields for the VS_2 nanosheet are higher than those on Si substrate and the values are 1.8 and 3.2 $V\mu m^{-1}$, respectively. We think that different substrates lead to different contact performance and further lead to different turn on fields and threshold fields. Better mechanical adhesion and electrical contact between nanosheets and substrates allow

efficient electron injection and transmission through VS_2 nanosheets.[35] Moreover, the values of turn-on fields and threshold fields for the concave and convex samples are all similar to those of flat sample. The linear F–N plots are also quite similar, as shown in the upper inset of Fig. 7a. The bent or unbent structures have no significant influence to the FE properties may be due to the high electrical conductivity and abundant sharp edges of VS_2 nanosheets. Their field enhancement factors were calculated and the values are all about 5020 for these three samples.

The current stability curve of flexible VS_2 concave emitter is given in Fig. 7b with original emission current density of 0.4 $mAcm^{-2}$. Compared with the current stability of Si substrate coated with VS_2 nanosheets shown in Fig. 6, the emission of the flexible emitters is similar to Si substrate, which indicates that the VS_2 nanosheet has beautiful current stability on flexible substrate without incurring a reduction in the current density under several times of bending conditions. The right inset of Fig. 7b shows the field emission images of the concave sample operated at an electric field of 3.2 $V\mu m^{-1}$. The emission spot density is similar to VS_2 nanosheets on Si substrate, but the brightness is a bit lower.

4. Conclusions

In summary, VS_2 nanosheets were synthesized by a hydrothermal method and then ZnO nanoparticles were successfully combined with VS_2 by using deposition method through a thermal annealing process. The field emission properties of all the samples were measured and compared. It is demonstrated that the VS_2-ZnO metal-semiconductor junction can notably improve the field emission performance. The ZnO nanoparticles also played important roles in improving the properties for their small sizes and chemical stability. Owing to the good mechanical and high electrical conductivity of VS_2 nanosheets, the FE properties based on PET substrate are also remarkable and stable on bent or unbent conditions. We anticipate that VS_2 and VS_2-baesd nanomaterials would provide valuable insights for future field emission display applications, such as flexible displays.

Acknowledgments

The authors acknowledge financial support from the NSF of China (Grant Nos. 61204018 and 61274014), Innovation Research Project of Shanghai Education Commission (Grant No. 13zz033), Education Committee of Jiangsu Province (Grant No. 12KJD510011), and Nantong Application Program (Nos. BK2012039 and BK2012044).

Notes and references

[a] *Key Laboratory of Polar Materials and Devices (Ministry of Education of China), Department of Electronic Engineering, East China Normal University, Shanghai, 200241, P. R. China. Fax: +86-21-54345198; Tel: +86-21-54345198; E-mail: yk5188@263.net*

[b] *School of Electronics and Information, Nantong University, Nantong, 226019, P. R. China.*

1. R. R. Devarapalli, R. V. Kashid, A. B. Deshmukh, P. Sharma, M. R. Das, M. A. More and M. V. Shelke, *J Mater Chem C*, 2013, **1**, 5040.
2. D. Ye, S. Moussa, J. D. Ferguson, A. A. Baski and M. S. El-Shall, *Nano Lett*., 2012, **12**, 1265.
3. N. S. Xu and S. E. Huq, *Materials Science and Engineering: R: Reports*, 2005, **48**, 47.
4. C. Hernandez‐Garcia, M. L. Stutzman and P. G. O'Shea, *Physics Today*, 2008, **61**, 44.
5. K. Yu, Y. S. Zhang, F. Xu, Q. Li, Z. Q. Zhu and Q. Wan, *Appl. Phys. Lett.*, 2006, **88**, 153123.
6. H. Yin, M. Luo, K. Yu, Y. Gao, R. Huang, Z. Zhang, M. Zeng, C. Cao and Z. Zhu, *ACS Applied Materials & Interfaces*, 2011, **3**, 2057.
7. Z. R. Dai, Z. W. Pan and Z. L. Wang, *Adv Funct Mater*, 2003, **13**, 9.
8. K. S. Novoselov, *Science*, 2004, **306**, 666.
9. S. Stankovich, D. A. Dikin, G. H. B. Dommett, K. M. Kohlhaas, E. J. Zimney, E. A. Stach, R. D. Piner, S. T. Nguyen and R. S. Ruoff, *Nature*, 2006, **442**, 282.
10. N. Shang, P. Papakonstantinou, P. Wang, A. Zakharov, U. Palnitkar, I.-N. Lin, M. Chu and A. Stamboulis, *Acs Nano*, 2009, **3**, 1032.
11. Z. Xiao, J. She, S. Deng, Z. Tang, Z. Li, J. Lu and N. Xu, *Acs Nano*, 2010, **4**, 6332.
12. X. Wei, Y. Bando and D. Golberg, *Acs Nano*, 2011, **6**, 705.
13. W. Lei, C. Li, M. T. Cole, K. Qu, S. Ding, Y. Zhang, J. H. Warner, X. Zhang, B. Wang and W. I. Milne, *Carbon*, 2013, **56**, 255.
14. C. S. Rout, B.-H. Kim, X. Xu, J. Yang, H. Y. Jeong, D. Odkhuu, N. Park, J. Cho and H. S. Shin, *Journal of the American Chemical Society*, 2013, **135**, 8720.
15. M. Mulazzi, A. Chainani, N. Katayama, R. Eguchi, M. Matsunami, H. Ohashi, Y. Senba, M. Nohara, M. Uchida, H. Takagi and S. Shin, *Phys. Rev. B*, 2010, **82**, 075130.
16. J. Feng, L. Peng, C. Wu, X. Sun, S. Hu, C. Lin, J. Dai, J. Yang and Y. Xie, *Adv Mater*, 2012, **24**, 1969.
17. B. Van Laar and D. Ijdo, *J. Solid State Chem*., 1971, **3**, 590.
18. M. Yokoyama, M. Yoshimura, M. Wakihara, S. Somiya and M. Taniguchi, *J. Solid State Chem*., 1985, **60**, 182.
19. A. V. Murugan, C. S. Gopinath and K. Vijayamohanan, *Electrochemistry Communications*, 2005, **7**, 213.
20. J. Feng, X. Sun, C. Wu, L. Peng, C. Lin, S. Hu, J. Yang and Y. Xie, *Journal of the American Chemical Society*, 2011, **133**, 17832.
21. D. Gao, Q. Xue, X. Mao, W. Wang, Q. Xu and D. Xue, *J Mater Chem C*, 2013, **1**, 5909.
22. J. O. Hwang, D. H. Lee, J. Y. Kim, T. H. Han, B. H. Kim, M. Park, K. No and S. O. Kim, *J. Mater. Chem.*, 2011, **21**, 3432.
23. H. J. Jeong, H. Y. Kim, H. D. Jeong, S. Y. Jeong, J. T. Han and G.-W. Lee, *J. Mater. Chem.*, 2012, **22**, 11277.
24. C. Zhang, G. Wang, Y. Ji, M. Liu, Y. Feng, Z. Zhang and B. Fang, *Sensors and Actuators B: Chemical*, 2010, **150**, 247.
25. Q. F. Xu, J. N. Wang and K. D. Sanderson, *Acs Nano*, 2010, **4**, 2201.
26. J.-h. Deng, R.-t. Zheng, Y.-m. Yang, Y. Zhao and G.-a. Cheng, *Carbon*, 2012, **50**, 4732.
27. W. T. Zheng, Y. M. Ho, H. W. Tian, M. Wen, J. L. Qi and Y. A. Li, *The Journal of Physical Chemistry C*, 2009, **113**, 9164.
28. M. Li, F. Kong, L. Li, Y. Zhang, L. Chen, W. Yan and G. Li, *Dalton T*, 2011, **40**, 10961.
29. C. Ye, Y. Bando, X. Fang, G. Shen and D. Golberg, *The Journal of Physical Chemistry C*, 2007, **111**, 12673.
30. L. Li, X. Fang, H. G. Chew, F. Zheng, T. H. Liew, X. Xu, Y. Zhang, S. Pan, G. Li and L. Zhang, *Adv Funct Mater*, 2008, **18**, 1080.
31. R. Zou, G. He, K. Xu, Q. Liu, Z. Zhang and J. Hu, *J Mater Chem A*, 2013, **1**, 8445.
32. C. Wu, F. Li, Y. Zhang and T. Guo, *Carbon*, 2012, **50**, 3622.
33. J. Liu, B. Zeng, X. Wang, W. Wang and H. Shi, *Appl. Phys. Lett.*, 2013, **103**, 053105.
34. C.-C. Tang, X.-W. Xu, L. Hu and Y.-X. Li, *Appl. Phys. Lett.*, 2009, **94**, 243105.
35. I. Lahiri and W. Choi, *Acta Mater*, 2011, **59**, 5411.

Graphical Abstract

Multi-layered VS_2 nanosheets were synthesized via a facile hydrothermal process. Due to the large quantities of sharp edges, VS_2 nanosheets showed excellent field emission properties and the performance was further improved by ZnO nanoparticles coating on the surface of VS_2 nanosheets. Moreover, as a 2D flexible material, VS_2 nanosheets exhibit almost the same field emission properties in both bent and unbent conditions based on PET substrates.